Thomson Scattering Measurements of the Langmuir Wave Spectra Resulting from Stimulated Raman Scattering

K. L. Baker, R. P. Drake, B. S. Bauer, K. G. Estabrook, and A. M. Rubenchik
Plasma Physics Research Institute, University of California Davis and Lawrence Livermore National Laboratory, Livermore, California 94550

C. Labaune, H. A. Baldis, N. Renard, S. D. Baton, E. Schifano, and A. Michard
Laboratoire pour L'Utilisation des Lasers Intenses, Ecole Polytechnique, Palaiseau, France

W. Seka and R. E. Bahr
University of Rochester, Rochester, New York 14627
(Received 28 February 1996)

Thomson scattering was used to measure the Langmuir wave spectrum generated by stimulated Raman scattering. This experiment detected Langmuir waves with components both parallel and antiparallel to the incident laser's wave vector $\vec{k}_0$. The parallel component was attributed to stimulated Raman scattering. However, the Langmuir waves moving antiparallel to $\vec{k}_0$, which cannot be explained by stimulated Raman scattering, were attributed to the Langmuir decay instability. [S0031-9007(96)00605-9]

PACS numbers: 52.35.–q

The saturation of Langmuir waves in plasmas is an important issue in many applications involving plasmas. These applications include inertial confinement fusion [1], particle accelerators [2], current drive in tokamaks [3], and x-ray lasers [4]. In laser-produced plasmas, Langmuir waves may be driven by several instabilities, one of which is stimulated Raman scattering (SRS). In SRS, an incident electromagnetic wave resonantly drives a Langmuir wave and a scattered electromagnetic wave [5,6]. Much of the prior work on SRS has been focused on its onset, which proved difficult to understand [7–11]. Few experiments have looked directly for these saturation mechanisms [12–14]. Many recent simulations and analyses have indicated that the Langmuir decay instability may be responsible for the saturation of SRS [15–18]. The present work is, to our knowledge, the first experimental study of the three wave process known as the Langmuir decay instability in laser-produced plasmas.

The Langmuir decay instability involves the decay of a Langmuir wave into a second Langmuir wave and an ion acoustic wave. This instability can be driven by the Langmuir waves produced by stimulated Raman scattering, two plasmon decay, the ion acoustic decay instability, and other mechanisms as well. For the present experiment stimulated Raman scattering was chosen to provide the Langmuir pump wave. The electromagnetic daughter wave associated with stimulated Raman scattering is easily diagnosed for a direct comparison to the measured Langmuir waves. The primary Langmuir wave spectrum driven by stimulated Raman scattering is also much simpler than the primary spectrum driven by either the ion acoustic decay instability or two plasmon decay. Specifically, two plasmon decay and the ion acoustic decay instability generate Langmuir waves which have components both parallel and antiparallel to the incident laser wave vector. In contrast, stimulated Raman scattering only drives Langmuir waves with components in the same direction as the incident laser wave vector. Thus any Langmuir waves traveling antiparallel to the laser wave vector must be due to the Langmuir decay instability or another mechanism which can reverse the wave vector of the Langmuir wave.

The experiments were performed using the LULI laser at Ecole Polytechnique. The layout of the experiment is shown in Fig. 1. The plasma was formed by two counterpropagating 0.526 μm beams impinging upon a 1.2 μm thick, 440 μm diameter, CH foil. These $f/6$ plasma formation beams contained random phase plates with 0.75 mm elements which produced an approximate FWHM focal spot size on target of 360 μm. The $f/6$

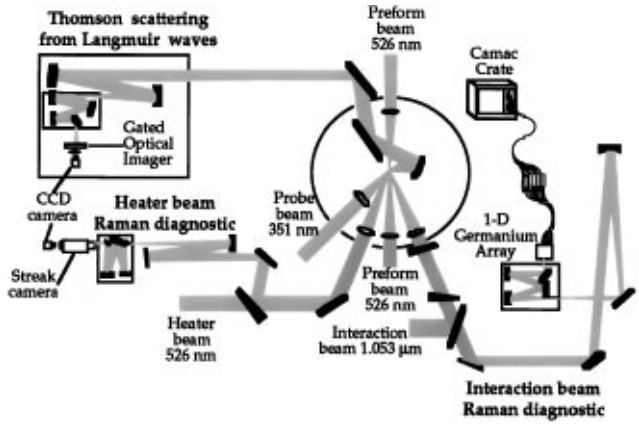

FIG. 1. Experimental setup showing the Thomson scattering diagnostic, as well as the stimulated Raman scattering diagnostics from the 526 nm heater beam and the 1 μm interaction beam.

heater beam at 0.526 μm and the $f/6$ interaction beam at 1.053 μm were delayed by 1.1 and 1.7 ns from the preform beams, respectively. The heater beam contained a random phase plate with 1.5 mm elements; however, a random phase plate was not used on the interaction beam.

Figure 2 shows data from the heater-beam Raman diagnostic with the timing of beams drawn to the right of the figure. The heater-beam Raman diagnostic is shown in Fig. 1. This diagnostic employed a 0.25 m spectrometer coupled through a streak camera to a charge coupled device detector, and produced data regarding experiment timing and plasma density. The features near $t = 0$ are produced by scattering from the two preform beams at 526 nm, and appear in both first and second order of the grating. The feature above 702 nm, driven from $t = 0.8$ to 1.25 ns, is produced by SRS of the heater beam. It provides a measurement of the decay of the maximum density of the plasma during this period. The feature at 702 nm, driven from $t = 1.2$ to 1.6 ns, is produced by Thomson scattering of the interaction beam from the Langmuir waves associated with two plasmon decay. (Two plasmon decay is driven by the interaction beam when densities between 20% and 25% of its critical density are present [19].) Finally, the feature above 750 nm, driven from $t = 1.45$ to 1.65 ns, is produced by Thomson scattering of the interaction beam from Langmuir waves at lower densities.

The temperature of the plasma was measured by collective Thomson scattering from thermal level ion acoustic waves [20]. This measurement placed the electron temperature between 400 and 500 eV with an interaction beam intensity around 5×10^{12} W/cm^2. Hydrodynamic simulations using LASNEX predict that higher interaction beam intensities would raise the electron temperature by approximately 200 eV.

The Thomson scattering probe beam at 351 nm was incident on the plasma approximately 1.4 ns after the plasma formation beams. The use of a 3 to 1 ratio for the probe beam frequency to interaction beam frequency allowed the Thomson downscattered signal from the Langmuir waves traveling in the same direction as the laser wave vector to be scattered at nearly the same angle as the Thomson upscattered signal from the Langmuir waves traveling in the opposite direction to the laser wave vector. These signals were relayed to a spectrometer for spectral dispersion. The Fourier transform plane was imaged onto the spectrometer slit and onto the gated optical imager providing a measurement of frequency versus wave number [13,21].

The measurement of the Langmuir wave spectra by Thomson scattering and the corresponding Raman spectrum are shown in Fig. 3. This figure was taken with a probe $f/\#$ of approximately 3.3 which allowed for a large sampling of the Langmuir wave wave-number spectrum. In Fig. 3(a), the longer wavelength feature represents the Thomson downscattered feature from the waves that copropagate with the laser, which we

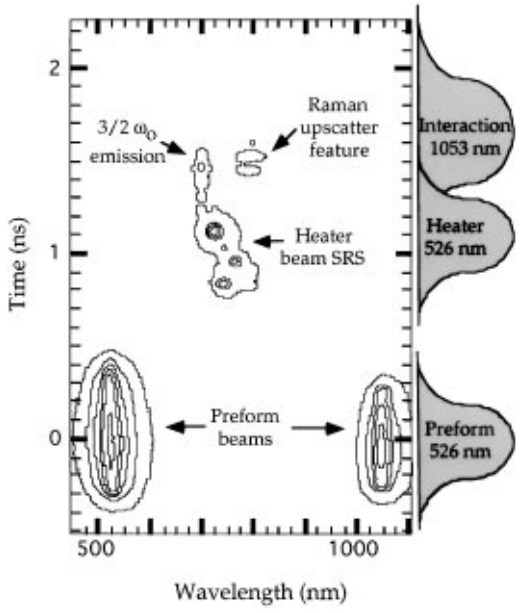

FIG. 2. Spectrum from the heater beam stimulated Raman scattering diagnostic. Relative beam timing is drawn along the right side. The vertical axis represents relative time, while the horizontal axis shows the wavelength of the scattered light. The contours represent factors of 2 in intensity.

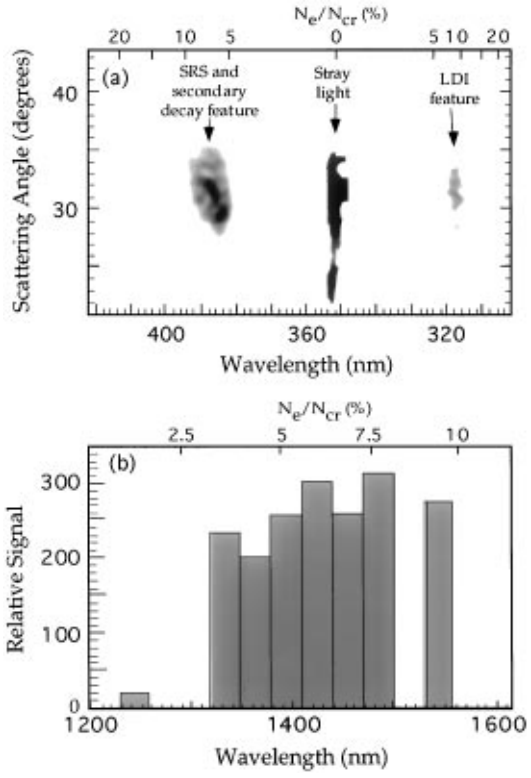

FIG. 3. Thomson scattering measurement of the Langmuir wave spectrum using a $f/3.3$ probe beam (a) and the backscattered electromagnetic waves (b) driven by the 1 μm interaction beam. The channels centered at 1275, 1305, and 1510 nm were not functional.

will refer to as SRS Langmuir waves [22]. The central feature at 351 nm is a combination of stray probe light and Thomson scattering from ion acoustic waves whose frequency shift is less than the resolution of the spectrometer. The shorter-wavelength feature represents Thomson scattering from Langmuir waves traveling opposite to the laser wave vector, which we will refer to as counterpropagating Langmuir waves. We have interpreted this feature as being due to the Langmuir decay instability, as discussed below. Figure 3(b) shows the corresponding, time-integrated measurement of the scattered electromagnetic waves driven by stimulated Raman scattering. These signals were measured by coupling the backscattered signal from the interaction beam through a 0.35 m spectrometer to a germanium photodiode array. The observed signals correspond very well to those one would expect from the SRS Langmuir waves shown in Fig. 3(a). Figure 4 displays the results from a separate shot in which an aperture was placed in front of the Thomson probe beam resulting in a $f/\#$ of approximately 25. The explanation of the features is the same as discussed for Fig. 3. In this case the measured signal was just above the detection threshold of the detector, which resulted in a reduced signal to noise ratio.

The measured ratio of the amplitude of the SRS Langmuir wave n_{LR}/n_{oe} to the amplitude of the counterpropagating Langmuir waves n_{LD}/n_{oe} is 0.5 ± 0.2. The coupled equations describing SRS and the Langmuir decay instability [17] can be used to infer the relationship between the amplitudes of the participating waves. With a CH plasma, the Landau damping on the ion acoustic waves is approximately 10% of the ion acoustic frequency [23] or $\mathrm{Im}[\omega_{iD}]/\mathrm{Re}[\omega_{iD}] \sim 0.1$. The strong damping approximation reduces the ion wave equation to an algebraic equation relating the ion wave amplitude to the product of the Langmuir pump and daughter wave amplitudes,

$$\frac{n_{iD}}{n_{oe}} \approx \frac{1}{2}\left(\frac{c_S k_{iD}}{\nu_{iD}}\right)\frac{1}{k_{LR}^2\lambda_{\mathrm{De}}^2}\left(\frac{n_{LR}}{n_{oe}}\,\frac{n_{LD}}{n_{oe}}\right), \qquad (1)$$

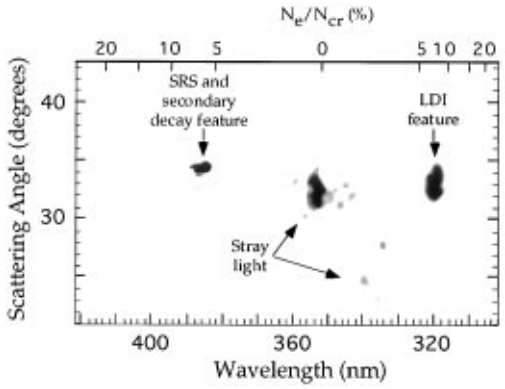

FIG. 4. Thomson scattering measurement of the Langmuir wave spectrum using a $f/25$ probe beam.

where k_{LR} is the SRS Langmuir wave number, n_{iD}/n_{oe} is the ion wave amplitude, λ_{De} is the Debye length, and $c_S k_{iD}/\nu_{iD}$ is the ratio of the real part of the frequency to the amplitude damping of the ion acoustic wave. c_S is the sound speed and k_{iD} is the wave number of the ion acoustic wave.

The Langmuir decay instability (LDI) can saturate the Raman process by increasing the damping on the Langmuir wave [17], making SRS go below threshold for absolute instability. The threshold for absolute instability is given by

$$\gamma_{OR} > 0.5\nu_{LR}\sqrt{\frac{V_{ER}}{V_{LR}}} \quad \text{where } \nu_{LR} \approx 0.5\omega_{pe}\left(\frac{n_{iD}}{n_{oe}}\,\frac{n_{LD}}{n_{oe}}\right), \qquad (2)$$

ω_{pe} is the plasma frequency, γ_{OR} is the homogeneous growth rate for Raman scattering, and V_{ER} and V_{LR} are the group velocities of the Raman scattered light wave and SRS Langmuir wave, respectively. The damping is due primarily to the pump depletion term in the SRS Langmuir wave equation. Upon combining Eqs. (1) and (2) in conjunction with the measured ratio of the pump Langmuir wave and the counterpropagating Langmuir wave, the SRS Langmuir wave's amplitude was inferred to be 0.05.

In order for the Langmuir decay instability to explain the results of this experiment, this amplitude must be above the convective threshold for LDI [18],

$$\gamma_{OD} > \sqrt{\nu_{LD}\nu_{iD}} \Rightarrow \frac{n_{LR}}{n_{oe}} > 4k_{LR}\lambda_{\mathrm{De}}\sqrt{\frac{\nu_{LD}}{\omega_{pe}}\,\frac{\nu_{iD}}{c_S k_{iD}}}, \qquad (3)$$

where ν_{LD} is the damping on the counterpropagating Langmuir wave. The homogeneous growth rate for the Langmuir decay instability is defined as $\gamma_{OD} \approx 0.25 \times \omega_{pi}(n_{LR}/n_{oe})(k_{iD}/k_{LD})\sqrt{\omega_{pe}/c_S k_{iD}}\,(\hat{e}_{LR}\cdot\hat{e}_{LD})$, where ω_{pi} is the ion plasma frequency, k_{LD} is the wave number of the LDI Langmuir wave, and $\hat{e}_{LR}$ and $\hat{e}_{LD}$ are unit vectors along the wave vectors of the SRS Langmuir wave and the LDI Langmuir wave, respectively. Ignoring the damping effects of cascading, the convective threshold for the Langmuir decay instability near 7% of critical is approximately $n_{LR}/n_{oe} = 0.005$. This amplitude is well below the value obtained above suggesting that the Raman Langmuir wave was above the damping threshold for Langmuir decay.

Other explanations for the counterpropagating Langmuir waves have been considered. The most straightforward way of producing counterpropagating Langmuir waves involves the propagation of the Langmuir waves produced by stimulated Raman scattering up the density gradient to their reflection point and back. This process damps the Langmuir waves far too much to explain the observed ratio of amplitudes. While very large ion waves might in principle produce densities large enough to directly reflect SRS Langmuir waves, this would require

large ion waves (~10%) which would likely quench the SRS itself [12]. The observed, counterpropagating Langmuir waves have the wrong wave number to have been produced by quasiresonant mode coupling with ion waves driven by stimulated Brillouin scattering [24,25]. The enhanced Thomson scattering model [8,26] would predict Langmuir waves traveling in both directions of the incident laser. According to the enhanced Thomson scattering model, Langmuir waves are produced by the bump-on-tail instability between hot electrons and the background electron distribution. The electromagnetic wave attributed to stimulated Raman scattering is assumed to be produced by scattering of the pump beam off these enhanced plasma waves. The enhanced Thomson scattering model would, however, predict a much broader spectrum of Langmuir waves than observed in this experiment [27].

In summary, the Langmuir wave spectra measured by Thomson scattering show that Langmuir waves are present which propagate both parallel and antiparallel to the laser wave vector. The Langmuir waves propagating parallel to the laser's wave vector are expected as they are being driven directly by stimulated Raman scattering. The counterpropagating waves are not predicted directly from the Raman process itself. A number of mechanisms were reviewed as possible candidates for the production of such waves; however, as discussed above these processes could not explain the data observed in the experiment. The presence and properties of the Langmuir waves traveling antiparallel to the incident laser's wave vector can be explained by the Langmuir decay of the Langmuir waves traveling parallel to the laser's wave vector, but not by any other mechanism identified above. This thus represents the first experimental observation of the Langmuir decay instability in laser-produced plasmas.

The authors would like to acknowledge useful discussions with D. M. Villeneuve, Russ Evans, T. W. Johnston, V. T. Tikhonchuk, and D. F. DuBois. The authors would also like to acknowledge the target fabrication group at the laboratory for laser energetics, in particular, Steven Noyse, for supplying the targets used in these experiments. Part of this work was performed under the auspices of the U.S. Department of Energy by the Lawrence Livermore National Laboratory under Contract No. W-7405-Eng-48.

[1] W. L. Kruer, Phys. Fluids B **3**, 2356 (1991).
[2] C. Joshi *et al.*, Nature (London) **311**, 525 (1984).
[3] J. H. Rogers *et al.*, Phys. Plasmas **7**, 1920 (1992).
[4] P. Amendt, D. C. Eder, and S. C. Wilks, Phys. Rev. Lett. **66**, 2589 (1991).
[5] W. L. Kruer, *The Physics of Laser Plasma Interactions* (Addison-Wesley Publishing Company, Inc., Redwood City, California, 1988).
[6] H. A. Baldis, E. M. Campbell, and W. L. Kruer, in *Handbook of Plasma Physics*, edited by A. Rubenchik and S. Witkowski (North-Holland, Amsterdam, 1991), p. 404.
[7] W. Seka *et al.*, Phys. Fluids **27**, 2181 (1984).
[8] A. Simon and R. W. Short, Phys. Rev. Lett. **53**, 1912 (1984).
[9] R. P. Drake *et al.*, Phys. Rev. Lett. **60**, 1018 (1988).
[10] H. C. Barr, T. J. M. Boyd, and A. P. Mackwood, Phys. Fluids B **4**, 2942 (1992).
[11] R. P. Drake, Laser Part. Beams **10**, 599 (1992).
[12] D. M. Villeneuve, H. A. Baldis, and J. E. Bernard, Phys. Rev. Lett. **59**, 1585 (1987).
[13] D. M. Villeneuve *et al.*, Phys. Rev. Lett. **71**, 368 (1993).
[14] F. Amiranoff *et al.*, Phys. Rev. Lett. **68**, 3710 (1992).
[15] G. Bonnaud, D. Pesme, and R. Pellat, Phys. Fluids B **2**, 1618 (1990).
[16] B. Bezzerides, D. F. DuBois, and H. A. Rose, Phys. Rev. Lett. **70**, 2569 (1993).
[17] T. Kolber, W. Rozmus, and V. T. Tikhonchuk, Phys. Fluids B **5**, 138 (1993).
[18] R. P. Drake and S. H. Batha, Phys. Fluids B **3**, 2936 (1991).
[19] W. Seka *et al.*, Phys. Fluids **28**, 2570 (1985).
[20] C. Labaune *et al.*, Phys. Rev. Lett. **75**, 248 (1995).
[21] D. M. Villeneuve *et al.*, J. Opt. Soc. Am. B **8**, 895 (1991).
[22] The downscattered feature may also include contributions from even number cascades in which further decay of the Langmuir waves driven by LDI reverses the direction of the Langmuir waves.
[23] E. A. Williams *et al.*, Phys. Plasmas **2**, 129 (1995).
[24] P. K. Kaw, A. T. Lin, and J. M. Dawson, Phys. Fluids **16**, 1967 (1973).
[25] H. C. Barr and F. F. Chen, Phys. Fluids **30**, 1180 (1987).
[26] A. Simon and R. W. Short, Phys. Fluids B **1**, 1073 (1989).
[27] K. L. Baker, Ph.D. dissertation, University of California at Davis, Davis, California, 1996.